11th Australasian Fluid Mechanics Conference
University of Tasmania, Hobart, Australia
14-18 December 1992

INSTABILITY IN VARIABLE DENSITY ROUND JETS

Murray RUDMAN[1], Ralf J. GATHMANN[2] and Marcel LESIEUR[2]

[1]CSIRO Division of Building Construction & Engineering, PO Box 56, Highett, VIC 3190, AUSTRALIA

[2]Institut de Mecanique de Grenoble, BP 53X, 38041 Grenoble Cedex, FRANCE

ABSTRACT

The stability of weakly compressible (Convective Mach number ≈ 0.3) three-dimensional round jets and their transition to turbulence is studied by means of a Direct Numerical Solution (DNS) technique. Temporal simulations are performed for axisymmetric jets with jet-centerline to ambient density ratios in the range 1 to 1/8. Added to each component of the initial jet velocity profile is a small random perturbation with an *rms* value of 0.3% of the jet-centerline velocity. The white noise perturbation allows the most unstable mode to grow naturally (under the constraint of enforced streamwise periodicity). Isosurface visualisation of two-point pressure correlations is introduced which allows the nature of the instability to be investigated more easily.

INTRODUCTION

The stability of axisymmetric jets have been investigated extensively (e.g., Michalke and Herman 1982, Monkewitz and Sohn 1988 and Martin and Meiburg 1991). The ratio of jet-centerline to ambient density, (S), is an important parameter in determining the stability regimes of the round jet. According to Monkewitz and Sohn (1988), in jets with a top-hat density profile and zero Mach number the first azimuthal mode is absolutely unstable when S is smaller than approximately 0.35 and the axisymmetric mode is absolutely unstable for S less than approximately 0.66. Absolute instability is thought to be the cause of self-sustaining global oscillations observed experimentally, (Sreenivasan et al. 1989, Riva et al. 1989, Monkewitz et al. 1990).

The effect of global density ratio on the non-linear regime of the instability and subsequent transition to turbulence is not well known and the numerical investigation performed here allows these regimes to be investigated. The stability calculations of Michalke and Hermann and Monkewitz and Sohn have been performed assuming the jet flow to be locally parallel. Similarly, in the calculations performed here the flow is initially parallel. In addition, the streamwise boundary conditions are periodic allowing the temporal evolution of the instability to be studied. The periodic boundary conditions enforce a length scale on the calculation and thus the results cannot be directly compared to the stability analyses.

NUMERICAL METHOD

The choice of numerical method is crucial for the success of direct numerical simulations. The code used here (see Gathmann and Chollet (1991)) is based on the piecewise parabolic method (PPM) of Collela and Woodward (1984) in combination with the linearised Riemann solver of Roe (1981). The scheme performs well in advection dominated problems and handles travelling waves very accurately. The diffusive source terms are included in an additional operator and are combined with the PPM scheme using time-splitting.

The Equations

The equations of motion written in conservative form are

$$\frac{\partial \mathbf{W}}{\partial t} + \nabla\cdot\mathbf{F}(\mathbf{W}) = \mathbf{S}(\mathbf{W}), \tag{1}$$

where

$$\mathbf{W} = \begin{bmatrix} \rho \\ \rho\mathbf{U} \\ \rho E \\ \rho Y \end{bmatrix}, \qquad \mathbf{F}(\mathbf{W}) = \begin{bmatrix} \rho\mathbf{U} \\ \rho\mathbf{U}\mathbf{U} + P \\ (\rho E + P)\mathbf{U} \\ \rho Y\mathbf{U} \end{bmatrix},$$

$$\mathbf{S}(\mathbf{W}) = \begin{bmatrix} 0 \\ \frac{1}{Re}\nabla\cdot(\mu\tau) \\ \frac{1}{Pr\,Re}\nabla\cdot(\kappa\nabla T) + \frac{1}{Re}\nabla\cdot(\mu\mathbf{U}\cdot\tau) \\ \frac{1}{Sc\,Re}\nabla\cdot(D\nabla Y) \end{bmatrix},$$

$$E = \frac{1}{2}\mathbf{U}\cdot\mathbf{U} + \frac{C_V}{M}T, \tag{2}$$

$$\tau_{ij} = \frac{\partial U_j}{\partial x_i} + \frac{\partial U_i}{\partial x_j} - \frac{2}{3}\delta_{ij}\frac{\partial U_k}{\partial x_k} \tag{3}$$

and Y is the mass fraction of jet fluid, used to allow easy visualisation of the jet. The viscosity is given by a Sutherland law,

$$\mu = \mu_0 T^{\frac{3}{2}}\frac{1.4}{T + 0.4}. \tag{4}$$

The Reynolds number is based on the jet diameter, ($2R$), and values of velocity, density and viscosity at the centre of the jet shear zone. The Mach number is based on values of velocity and sound speed at the centre of the shear zone. Defined in this way, the Mach number is almost equivalent to the convective Mach number of Papamoschou and Roshko (1984). The Prandtl and Schmidt numbers are set to unity and the thermal and species diffusion coefficients (κ and D) follow similar laws to the viscosity, equation 4.

Initial and boundary conditions

The calculations are performed on a $60 \times 44 \times 44$ grid with dimensions of $8 \times 3.5 \times 3.5$. The initial jet profile is that used by Michalke and Herman (1982) with zero co-flow. The profile is parameterised by R/θ and is

$$U(r) = \frac{U_0}{2}\left(1 - \tanh\left[\frac{1}{4}\frac{R}{\theta}\left(2r - \frac{1}{2r}\right)\right]\right), \quad (5)$$

where U_0 is the jet centerline velocity, R is the radius at which $U(r) = U_0/2$, and θ is the momentum boundary layer thickness. To a good approximation in the potential core, (Crighton and Gaster 1976),

$$\frac{R}{\theta} \approx 100/(3x/R + 4), \quad (6)$$

where x is the downstream distance from the jet exit. This relation gives a value of $R/\theta = 25.0$ at the jet outflow. An initial value of $R/\theta = 15.0$ is used here as a result of grid resolution constraints. Superimposed on the velocity profile (5) is a random perturbation to all three velocity components with a maximum amplitude of 0.5% of the jet-centerline velocity. The mass fraction of jet fluid (Y) is distributed in a similar way to eqn. (5) with a value of 1 at the jet centerline and zero in the free stream. The initial density distribution also has a similar profile to (5) modified by the Crocco-Busemann relation (see Schlichting 1979, Chapt. XIII). The initial pressure is constant everywhere.

The streamwise boundary conditions are periodic and the radiation side wall boundary conditions admit no incoming travelling waves.

RESULTS

A Reynolds number of 2000 and Mach number of 0.3 were used for all numerical simulations and calculations were performed on a Silicon Graphics Indigo workstation. To visualise the development of the instability into the non-linear regime iso-surface visualisation software developed at CSIRO is used. Iso-surfaces of constant Y (initially a cylindrical surface) give an indication of the region occupied by the jet fluid and are the light coloured surfaces in figures 1 and 2. Iso-surfaces of low pressure indicate where pressure fluctuations occur and once the instability has developed are well correlated with regions in the flow containing high vorticity. Pressure iso-surfaces are dark coloured surfaces in figures 1 and 2.

Development of the Instability

Figure 1 shows a time sequence of the development of the instability for the constant density jet. The initial instability appears to contain a component of the axisymmetric mode (or $m = 0$ mode) as seen in the pressure structures observed at $t = 2.0$ and 6.0. However it should be noted that these structures are often crescent shaped and their axis is often inclined to the axis of the jet. At $t = 2.0$ vortex lines are well-aligned with the low pressure structures. By $t = 6.0$ the ring like structures have grown in size and the first azimuthal modes, ($m = \pm 1$ modes), are clearly emerging especially in the left side of the jet. At $t = 8.0$ the predominant pattern is one of two counter rotating spirals as seen in the typical 'arms and legs' pattern in the

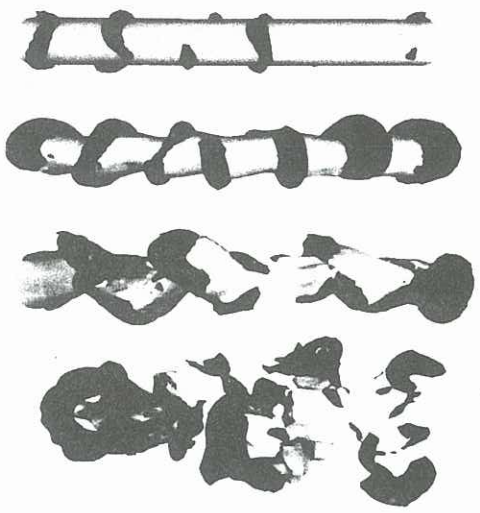

Figure 1: Development of jet instability for $S = 1$. (Iso-surfaces of: Y (light) and Low pressure (dark). Times $t = 2.0$, 6.0, 8.0 and 12.0.

low-pressure structures at this time. Iso-surfaces of positive and negative streamwise vorticity are well correlated with the low-pressure structures and occur in alternating positive/negative pairs down the length of the jet. The form of the pairing is consistent with initially axisymmetric structures having tilted alternately, eventually joining. The vortex lines also follow a similar pattern, suggesting the same mechanism. At $t = 12.0$ several hairpin structures are all that are left of the spirals and are still well correlated with regions of high vorticity. This evolutionary sequence was also observed by Fouillet (1991).

The development of the instability for the jet with S=1/8 is displayed in figure 2. The evolution is similar with an apparent axisymmetric component at early times. This is followed by the appearance of $m = \pm 1$ modes and later time hairpin structures. The same general sequence is also observed for $S = 1/2$ and $1/4$.

Two-point Pressure Correlations

A better understanding of the nature of the jet instability can be obtained from two-point pressure fluctuation correlations. The pressure fluctuation is defined as

$$P'(\mathbf{x}_r) = P(\mathbf{x}_r) - P(r) \quad (7)$$

where r is the distance from the point $\mathbf{x}_r$ to the jet centerline and $P(r)$ is the average pressure at this radius. For a position $\mathbf{x}_r$ and separation vector $\delta\mathbf{x} = \delta r\mathbf{e}_r + \delta\theta\mathbf{e}_\theta + \delta z\mathbf{k}$, the two-point correlation is defined to be

$$C(\mathbf{x}_r, \delta\mathbf{x}) = P'(\mathbf{x}_r)P'(\mathbf{x}_r + \delta\mathbf{x}). \quad (8)$$

A single radius, r, is chosen and $C(\mathbf{x}_r, \delta\mathbf{x})$ calculated for one $\mathbf{x}_r$ and each possible separation $\delta\mathbf{x}$. The calculation is repeated for each $\mathbf{x}_r$ in the cartesian grid that is r distant from the centerline and the results averaged to give the average correlation, $C(\delta\mathbf{x})$, for a separation $\delta\mathbf{x}$. Iso-surfaces of $C(\delta\mathbf{x})$ for $r = 0.5$ are plotted in figure 3 for $S = 1$ and figure 4 for $S = 1/8$.

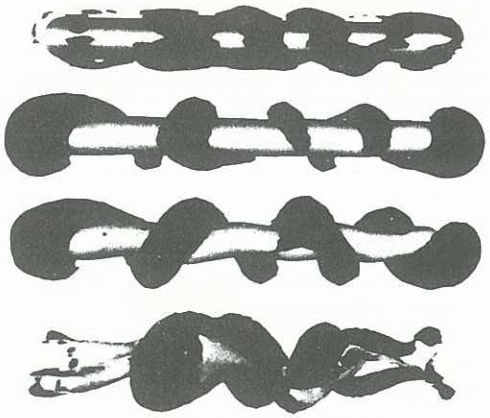

Figure 2: Development of jet instability for $S = 1/8$. (Iso-surfaces of: Y (light) and Low pressure (dark). Times t = 3.0, 8.0, 12.0 and 20.0

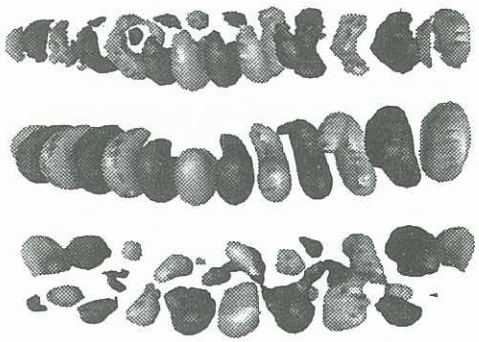

Figure 3: Two-point pressure correlations for $S = 1$. Positive correlation (light), Negative correlation (dark). Times t = 2.0, 6.0 and 8.0

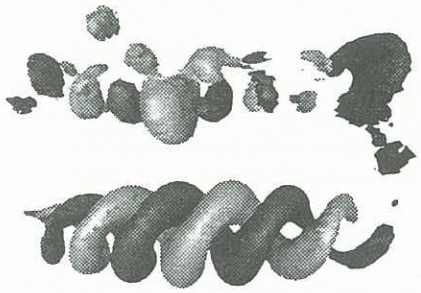

Figure 4: Two-point pressure correlations for $S = 1/8$. Positive correlation (light), Negative correlation (dark). Times t = 3.0, and 12.0

There is a strong axisymmetric component to C in figure 3 at t = 2.0. The crescent-like structures clearly show good correlation with a streamwise wavelength of 4/3. As the instability develops, the crescents decrease in angular extent and by t = 6.0 form a pattern of spiraling 'kidney-shaped' surfaces. The $m = \pm 1$ modes are becoming evident at this time. Because no clear pattern emerges in this particular computation the iso-surfaces of C become less regular, although the $m = \pm 1$ mode is still seen at t = 8.0 in the alternating surfaces of positive and negative correlation. The growth of the instability inferred from figures 1 and 3 is for the axisymmetric mode to grow faster in the early evolution of the instability and for the first azimuthal mode to take over as the jet enters the non-linear regime. However there is no clear delineation between the modes in the development of the instability. This is consistent with the theoretical findings of Michalke and Hermann (1982) which show that the two modes have similar growth rates near the jet outflow, and suggests that both modes are growing naturally at early times in the constant density jet here.

For $S = 1/8$ the early time correlation iso-surfaces are predominantly the $m = \pm 1$ modes as may be seen in figure 4 at t = 3.0. The pressure correlation along the jet centerline (not shown) gives a primary wavelength of 2.0. As the instability develops, a double spiral pattern emerges which is exceptionally clear by t = 12.0, the remnants of which are still visible at t = 25.0. The formation of such a clear double spiral indicates that one of the first azimuthal modes (either $m = +1$ or -1) dominates the other at this time. If both $m = \pm 1$ were of similar strength the pattern would be an alternating series of oppositely shaded surfaces, as is partially evident in figure 4 at t = 3.0. Although this calculation was not continued past t = 25.0, on the basis of the results for $S = 1/2$ and $1/4$ it is assumed that both $m = \pm 1$ modes arise. Thus for a $S = 1/8$ the first azimuthal mode appears to be stronger than the axisymmetric considerably earlier in the instability.

When $S = 1/2$ and $1/4$, the development is similar to $S = 1$, with the $m = 0$ mode growing more rapidly initially and the $m = \pm 1$ modes dominating at later times. The spiral two-point pressure correlation surfaces that develop evolve into a pattern consistent with both $m = \pm 1$ modes being present.

Quantitative Aspects

Because of the enforced streamwise periodicity, the wavelength of the fastest growing mode will depend on the length of the computational domain. The domain here is chosen to ensure several wavelengths are included to allow free interaction of adjacent structures. Bearing this constraint in mind, the wavelength of the fastest growing mode appears to decrease with decreasing S, i.e. hotter jets have a larger natural spatial wavelength in the temporal calculations. For $S = 1$ and $S = 1/2$, $\lambda_{max} = 1.33$, for $S = 1/4$, $\lambda_{max} = 1.6$ and for $S = 1/8$, $\lambda_{max} = 2.0$.

A measure of the growth rate of the instability is obtained by integrating the one-point velocity correlation (referred to as the fluctuating kinetic energy, $(E = \mathbf{U}' \cdot \mathbf{U}')$) over the computational domain. The results are shown in figure 5. The temporal growth rate of the total fluctuating kinetic energy decreases with decreasing density ratio as does the temporal growth rate of $(\overline{Y'Y'})$ (not shown).

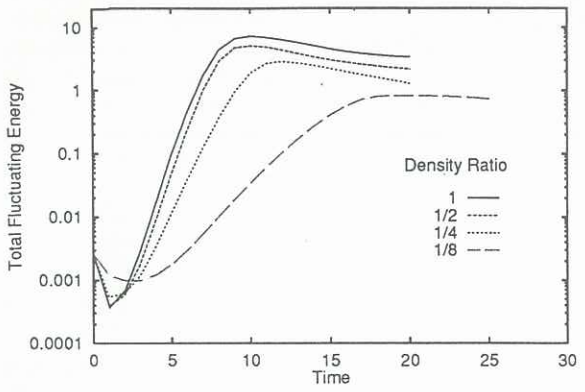

Figure 5: Growth of $E = (U'U')$ versus time for $S = 1, 1/2, 1/4$ and $1/8$.

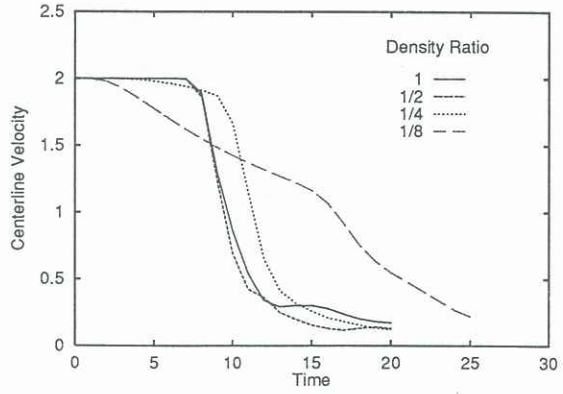

Figure 6: Average centerline velocity for $S = 1, 1/2, 1/4$ and $1/8$.

The temporal growth of these quantities here corresponds in some sense to their spatial growth in the physical jet and suggests that decreasing S decreases the instability growth rate. One possible explanation for this effect is that the initial kinetic energy, (which scales as the jet density), is considerably lower in the heated jets and coupled with the increased viscosity there results in lower growth rates. However, this observation is contrary to the enhanced spreading observed experimentally in heated jets (Monkewitz et al. 1990) and remains an unresolved point.

Except for $S = 1/8$, average jet centerline velocities given in figure 6 show a slow decline and then a sharp decrease once the instability becomes non-linear. The sharp decline corresponds to the region at the end of the potential core. The calculation with $S = 1/8$ was also performed with constant viscosity and indicated that the different nature of the centerline velocity here is due primarily to the effects of large jet viscosity.

CONCLUSIONS

The development of natural instability in the axisymmetric jets investigated here does not appear to be significantly affected by global density ratio except possibly for $S = 1/8$. Initially, for values less than $1/8$, the axisymmetric mode grows most rapidly but is soon overtaken by the first azimuthal mode. For the jet with $S = 1/8$ the first azimuthal mode appears to dominate throughout the calculation. The qualitative aspects of the later development are similar in all cases and follow the pattern shown in figures 1 and 2.

At no time were the creation of long lasting vortex rings and their pairing observed, contrary to experimentally observed, spatially developing jets. Although theoretical analysis suggests that the $m = 0$ and 1 modes have similar growth rates, the nature of experimental set-ups would favour axisymmetric perturbations rather than the totally random perturbations used here to initiate the growth of the instability. Calculations with pure axisymmetric and axisymmetric plus random perturbations are currently in progress.

Acknowledgements - One of the authors (MR) would like to thank Y. Fouillet and G. Binder of LEGI/IMG for many helpful interactions during his visit in 1991.

REFERENCES

COLELLA, P and WOODWARD P.R. (1984) The Piecewise Parabolic Method (PPM) for Gas-Dynamics Simulations. J Comp.Phys. 54, 174-201.

CRIGHTON, D.G. and GASTER, M., (1976) Stability of slowly diverging jet flow, J. Fluid Mech. 77, 397-413.

FOUILLET, Y. (1991) Numerical experiments relating to free-shear flows: effects of compressibility, These de l'Institut National Polytechnique de Grenoble.

GATHMANN, R.J. and CHOLLET, J-P., (1991) Direct Numerical Simulation of Supersonic Turbulent Combustion. Proc 4^{th} Int Symp in Computational Fluid Dynamics, Davis California.

MARTIN, J.E. and MEIBURG, E. (1991) Numerical investigation of three-dimensionally evolving jets subject to axisymmetric and azimuthal perturbations. J. Fluid Mech. 230, 271-318.

MICHALKE, A. and HERMAN, G. (1982) On the inviscid instability of a circular jet with external flow. J. Fluid Mech. 114, 343-359.

MONKEWITZ, P.A. and SOHN, K.D. (1988) Absolute Instability in Hot Jets. AIAA Journal 26, 911-916.

MONKEWITZ, P.A., BECHERT, D.W., BARISKOW, B. and LECHMANN, B. (1990) Self-excited oscillations and mixing in a heated round jet, J. Fluid Mech. 213, 611-639.

PAPAMOSCHOU, D. and ROSHKO,A. (1988) The compressible turbulent shear layer: an experimental study, J. Fluid Mech. 197, 543-577.

ROE, P.L. (1981) Approximate Reimann Solvers, Parameter Vectors, and Difference Schemes, J. Comp. Phys. 43 , 357-372.

RIVA, G., BINDER, G., TARDU, S. and FAVRE-MARINET, M. (1989) Turbulence 89: organized structures and turbulence in fluid mechanics. Eds. Lesieur, M. and Metais, O., Grenoble 18-21 September 1989, Kluwer Academic Publishers.

SCHLICHTING, H. (1979) Boundary-Layer Theory (seventh edition), McGraw-Hill New York.

SREENIVASAN, K.R., RAGHU, S. and KYLE, D. (1989) Absolute instability in variable density round jets. Exp. Fluids 7, 309-317.